Lasers in Surgery and Medicine 39:494–503 (2007)

Treatment of Cutaneous Vascular Lesions Using Multiple-Intermittent Cryogen Spurts and Two-Wavelength Laser Pulses: Numerical and Animal Studies

Wangcun Jia, PhD,[1]* Bernard Choi, PhD,[1] Walfre Franco, PhD,[1] Justin Lotfi, BS,[1] Boris Majaron, PhD,[3] Guillermo Aguilar, PhD,[1,2] and J. Stuart Nelson, MD, PhD[1]

[1]*Beckman Laser Institute, University of California, Irvine, California 92612*

[2]*Department of Mechanical Engineering, University of California, Riverside, California 92521*

[3]*Jožef Stefan Institute, Ljubljana, Slovenia*

Background and Objectives: Presently, cutaneous vascular lesions are treated using a single cryogen spurt and single laser pulse (SCS-SLP), which do not necessarily produce complete lesion removal in the majority of patients. In this study, the feasibility of applying multiple cryogen spurts intermittently with multiple two-wavelength laser pulses (MCS-MTWLP) was studied using numerical and animal models.

Study Design/Materials and Methods: Two treatment procedures were simulated: (1) SCS+532 nm SLP; and (2) MCS+532/1064 nm MTWLP. Light transport and heat diffusion in human skin were simulated with the Monte Carlo method and finite element model, respectively. Possible epidermal damage and blood vessel photocoagulation were evaluated with an Arrhenius-type kinetic model. Blood vessels in the rodent window chamber model (RWCM) were irradiated with either SLP or MTWLP. Laser-induced structural and functional changes in the vessels were documented by digital photography and laser speckle imaging (LSI).

Results: The numerical results show that the MCS-MTWLP approach can provide sufficient epidermal protection while simultaneously achieving photocoagulation of larger blood vessels as compared to SCS-SLP. Animal studies show that MTWLP has significant advantages over SLP by inducing irreversible damage to larger blood vessels without adverse effects.

Conclusions: MCS-MTWLP may be a promising approach to improve therapeutic outcome for patients with cutaneous vascular lesions featuring large blood vessels. Lasers Surg. Med. 39:494–503, 2007. © 2007 Wiley-Liss, Inc.

Key words: cryogen spray cooling; multiple cryogen spurts; multiple laser pulses; dual wavelength; laser dermatologic surgery; vascular malformation; port wine stain; Monte Carlo; bio-heat transfer

INTRODUCTION

Successful laser treatment of cutaneous vascular lesions, e.g., port wine stains (PWS) and telangiectasia, is based on photocoagulation of subsurface-targeted blood vessels without inducing thermal damage in the normal overlying epidermis. Although cryogen spray cooling (CSC) significantly enhances epidermal protection and allows the delivery of higher light dosage [1–3], large blood vessels can only be partially coagulated with the single cryogen spurt and single laser pulse (SCS-SLP) approach because blood in the center of the lumen is inadequately heated due to the strong light absorption by hemoglobin [4–6]. As a result, these partially coagulated vessels subsequently recanalize [7], which explains why current laser therapy results in a poor therapeutic outcome in lesions featuring large vessels [8–10].

New approaches to improve laser therapy of cutaneous vascular lesions have been investigated. Verkruysse et al. [11] have shown theoretically that multiple laser pulses can significantly increase the targeted blood vessel temperature as a result of cumulative heat propagation from adjacent vessels being heated simultaneously. Using numerical models, Aguilar et al. [12] demonstrated the application of multiple cryogen spurts intermittently with multiple laser pulses to overcome excessive epidermal heating for darkly pigmented patients. Jia et al. [13] numerically showed the feasibility to improve PWS

Abbreviations used: CSC, cryogen spray cooling; LSI, laser speckle imaging; MCS-MTWLP, multiple cryogen spurts and multiple two-wavelength laser pulses; NC, natural convection; PWS, port wine stain; RWCM, rodent window chamber model; SCS-SLP, single cryogen spurt and single laser pulse. The CSC methodology described in this article is contained within U.S. patent no. 5,814,040—Apparatus and Method for Dynamic Cooling of Biological Tissue for Thermal Mediated Surgery, awarded to J. Stuart Nelson, MD, PhD, Thomas E. Milner, PhD, and Lars O. Svaasand, PhD, and assigned to the Regents of the University of California. This work was presented in part at the annual meeting of the American Society for Laser Medicine and Surgery, April 2006, in Boston, MA.

Contract grant sponsor: National Institutes of Health; Contract grant numbers: GM 62177, AR 48458, AR 47551, HD42057; Contract grant sponsor: Laser Microbeam and Medical Program; Contract grant number: P41-RR01192; Contract grant sponsor: American Cancer Society; Contract grant number: ACS-IRG 98-279-04; Contract grant sponsor: UCR Academic Senate Grant.

*Correspondence to: Wangcun Jia, PhD, Beckman Laser Institute, 1002 Health Sciences Road East, Irvine, CA 92612-1475. E-mail: wjia@uci.edu

Accepted 25 May 2007
Published online 23 July 2007 in Wiley InterScience (www.interscience.wiley.com).
DOI 10.1002/lsm.20524

laser therapy by bulk skin preheating prior to CSC. Lasers operating at a wavelength of 532 or 1,064 nm in multi-pulse mode [14,15] significantly reduce lower extremity telangiectasia with a low incidence of long-term side effects, and achieved better results than the single-pulse mode.

Herein, we investigated the feasibility and benefit of treating cutaneous vascular lesions using multiple cryogen spurts applied intermittently with multiple two-wavelength (combined 532 and 1,064 nm) laser pulses (MCS-MTWLP). We hypothesized that MCS-MTWLP avoids the inherent risk of damaging the epidermis because the epidermis is actively cooled between successive MTWLP. Moreover, we assumed heat accumulation in large blood vessels with each successive laser pulse would result in higher core intravascular temperatures over longer periods of time. The addition of the 1,064 nm wavelength may directly contribute to irreversible vessel damage because of enhanced infrared absorption of blood after 532 nm exposure [16] as well as bulk dermal heating. In the present study, numerical models were used to investigate the effects of skin pigmentation, blood vessel size, and depth on photocoagulation induced by MCS-MTWLP. Irradiations with SLP and MTWLP of in vivo blood vessels in an animal model were also conducted.

STUDY DESIGN/MATERIALS AND METHODS

Numerical Models

Details of the numerical models have been discussed in [13]. In brief, there are three main components: (1) a Monte Carlo light distribution model; (2) a finite element heat diffusion model; and (3) an Arrhenius rate process integral to calculate thermal damage. The Monte Carlo model simulates light transport to produce energy deposition in model skin during pulsed laser exposure. The finite element model simulates heat transfer in skin during CSC, pulsed laser irradiation, and thermal relaxation phases to compute the time-dependent temperature distribution within model skin. The Arrhenius rate process integral calculates the tissue denaturation ratio, Ω. The damage threshold for tissue necrosis is selected as $\Omega = 1$ (a 63% decrease from the original total of undamaged tissue constituents).

The skin is modeled as two infinitely wide layers representing the epidermis and dermis with thickness of 60 and 4940 μm, respectively. Six vessels with diameters ranging from 50 to 150 μm were simulated in the dermis (see Fig. 1); two vessel depths of 300 and 800 μm were studied. Lateral distances between vessels were sufficient large so that heat diffusion between vessels can be neglected during the simulated treatment period.

The optical properties of skin and blood at a wavelength of 532 nm (Table 1) are from [17] except the epidermal absorption coefficient (Table 2), which was derived from the threshold radiant exposure for immediate epidermal denaturation [18,19]. Optical properties of skin at the 1,064 nm wavelength listed in Table 3 are bulk optical properties of fresh porcine dermis determined by combining surface roughness, reflectance, and transmittances with Monte Carlo-based inverse calculations [20]. These properties are much different from those determined without consideration of surface roughness [21]. The blood absorption coefficient was calculated from the extinction coefficients [22] for hemoglobin and oxyhemoglobin by assuming a 45% hematocrit and 80% oxygenation. The scattering coefficient and anisotropic factor of blood listed in Table 3 were determined at 960 nm [23].

The thermo-physical properties of each skin component and blood are the same as those in [13]. The initial skin temperature is 35°C. The simulated sequence of SCS-SLP consists of a cryogen spurt and a 532 nm laser pulse followed by natural convection (NC). The simulated sequence of MCS-MTWLP consists of two pairs of cryogen spurts and combined 532 and 1,064 nm laser pulses followed by NC. The thermal boundary conditions during the cryogen spurt and NC are the same as those in [13]. Heat transfer owing to blood perfusion was neglected because that effect is not critical during the short time scales (i.e., hundreds of milliseconds) considered in this study [24]. The latent heat of tissue water vaporization was assumed to be effective specific heat, $c_{\text{eff}} = (c + D \cdot \Delta H)$, where c is the specific heat of water. ΔH is the latent heat

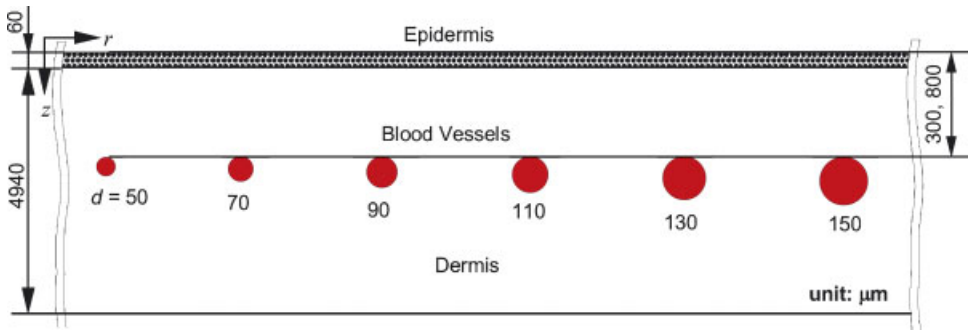

Fig. 1. Geometries of human skin model with discrete blood vessels (not to scale). Numbers to the left and right in the figure are also in micrometer. [Figure can be viewed in color online via www.interscience.wiley.com.]

TABLE 1. Optical Properties of Various Skin Components Used at 532 nm

Skin component	μ_a (1/mm)	μ_s (1/mm)	g
Epidermis	See Table 2	53.0	0.77
Dermis	0.27	15.6	0.77
Blood	26.6	47.3	0.99

of vaporization, and D is defined as a normalized Gaussian pulse (having unity integral), according to the following equation

$$D = \frac{\exp\left(-(T - T_B)^2/\Delta T^2\right)}{\sqrt{\pi \Delta T^2}} \quad (1)$$

where T_B is the temperature at which the rate of water vaporization is maximal. We assume $T_B = 108^\circ C$ to account for blood superheating before vaporization. $\Delta T = 2.5^\circ C$, which does not significantly affect the simulated temperature field, is selected arbitrarily.

The Arrhenius rate process integral is used to quantify tissue thermal damage:

$$\Omega(r,z,\tau) = \ln\left[\frac{C_n(r,z,0)}{C_n(r,z,\tau)}\right] = A\int_0^\tau \left\{\exp\left[-\frac{\Delta E}{RT(r,z,t)}\right]dt\right\} \quad (2)$$

where C_n is the remaining concentration of native tissue at exposure time t, τ is the total procedure time, and R is the universal gas constant (8.314 J/(mole · K)). We use values $A = 1.8\times10^{51}$ second^{-1} and $\Delta E = 327{,}000$ J/mole for bulk skin [25], and $A = 7.6\times10^{66}$ second^{-1} and $\Delta E = 455{,}000$ J/mole for blood [26]. Calculations of Ω are maintained for a period of time after laser irradiation until thermal damage accumulation has ceased.

In Vivo Animal Model

The rodent window chamber model (RWCM) [27–31] was used to study the laser-induced structural and functional changes in blood vessels. Briefly, the animal was anesthetized with a combination of ketamine and xylazine (4:3 ratio, 0.1 g/100 g body weight) administered by intraperitoneal injection. The dorsal skin was shaved and epilated then lifted and sutured to a C-clamp. A 12 mm circle of skin from one side was removed to expose the subdermis. A titanium chamber was bolted and sutured to both sides of the skin. A thin glass window was installed onto the chamber to protect the exposed subdermis, while offering an unobstructed view of the microvascular structure and blood flow dynamics. The protocol described herein for the RWCM was approved by the University of California, Irvine, Animal Care and Use Committee. Our preliminary studies using this model have shown that the RWCM is suitable for long-term, longitudinal analyses of microvascular-targeted laser therapy [31].

TABLE 2. Epidermal Absorption Coefficient, $\mu_{a,epi}$ (mm^{-1})

Subjects Wavelength λ (nm)	694[a]	532[b]	1,064
Moderately pigmented	0.9	2.61	0.31[c]
Darkly pigmented	2	5.79	0.36[b]

[a]Derived from the threshold radiant exposure for immediate epidermal whitening [18].
[b]Assume the $\mu_{a,epi} \sim \lambda^{-4}$ [19].
[c]The same as dermal absorption coefficient.

TABLE 3. Optical Properties of Dermis and Blood at 1,064 nm

Components	μ_a (1/mm)	μ_s (1/mm)	g
Dermis[a]	0.31	2.6	0.86
Blood	0.4[b]	50.5[c]	0.992[a]

[a]Takes surface roughness into consideration [20].
[b]45% hematocrit and 80% oxygenation [22].
[c]Wavelength is 960 nm [23].

Before irradiation, the animal was positioned with the subdermal side facing the laser. Thirteen blood vessels with diameters ranging between 137 and 200 μm were irradiated with a prototype Nd:YAG/KTP laser system (Dualis^{VP} Plus, Fotona, Ljubljana, Slovenia) which emits single or multiple pulses at wavelengths of 532 and 1,064 nm simultaneously. The laser radiant exposure at 1,064 nm is 1.8 times that at 532 nm. To obtain 532 nm SLP, we used an optical filter (10QM20HM, Newport, Irvine, CA) which blocked 1,064 nm light and had a transmittance of 94% at 532 nm. Laser-induced structural and functional changes were documented using digital photography and laser speckle imaging (LSI). For RWCM photography, we used a color CCD camera (MicroPublisher 3.3RTV, QImaging, Surrey, BC, Canada) equipped with a macro lens (1:1 magnification). To visualize RWCM blood flow, we used a monochromatic CCD camera (Retiga EXi, QImaging) to record speckle images generated by low-power continuous laser irradiation. In the absence of movement, the image has a static speckle pattern. However, the presence of a moving object inside the scattering medium, such as a red blood cell, leads to local blurring of the speckle pattern. A sliding-window-based algorithm was then used to convert raw speckle images to flow maps [30].

RESULTS

Simulated Temperature Distribution

In Figures 2 and 3, spatial and temporal temperature distributions are shown for moderately pigmented skin and blood vessels located 300 μm below the surface. For the SCS-SLP simulation, we assume a typical cooling period of 80 milliseconds, which includes a 50 milliseconds cryogen spray and a 30 milliseconds delay. The SLP has a duration of 1 millisecond and a radiant exposure of 5 J/cm^2, which is the simulated threshold for epidermal damage. For MCS-MTWLP, we also assume an initial cooling period of 80 milliseconds followed by two 1 millisecond TWLP at an

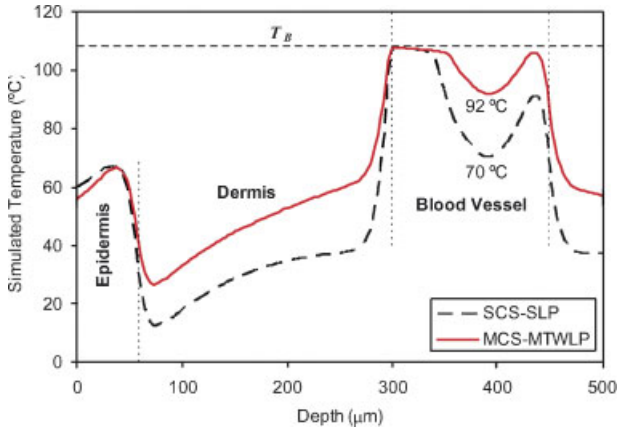

Fig. 2. Temperature profiles as a function of depth for SCS-SLP and MCS-MTWLP at the end of the single (dashed curve) or the second multiple (solid curve) laser pulses, respectively. Moderately pigmented skin; blood vessel depth, 300 μm; SLP, 5 J/cm^2; MTWLP, 4 J/cm^2 532 nm+6 J/cm^2 1,064 nm, repetition rate, 20 Hz. [Figure can be viewed in color online via www.interscience.wiley.com.]

interval of 49 milliseconds, which effectively provides a repetition rate of 20 Hz. The skin is actively cooled between the two pulses. The radiant exposures in the MTWLP simulation are 4 J/cm^2 and 6 J/cm^2 for 532 and 1,064 nm, respectively.

Figure 2 shows the temperature profiles as a function of depth along the longitudinal axis through the center of a 150 μm diameter blood vessel. The illustrated time point is the end of the SLP (dashed curve) or the second TWLP (solid curve). The temperature distribution in the epidermis with MCS-MTWLP is slightly lower as compared to SCS-SLP because of the lower 532 nm radiant exposure used with MTWLP. It should also be noted that the highest epidermal temperature is not located at the epidermal–dermal junction (i.e., basal layer) because we assume melanin is homogeneously distributed in the epidermis. The dermal temperature with MTWLP is higher as compared to SLP due to bulk skin heating by 1,064 nm which might lead to dermal damage if the radiant exposure is too high. Within the blood vessel, much higher temperature is achieved at the bottom portion of the lumen with MTWLP, albeit the temperatures in the top portion are similar for both SLP and MTWLP because water vaporization is assumed in our model.

Figure 3a shows the temperature variations over time in the epidermis at the position of maximum temperature increase for SCS-SLP (squares) and MCS-MTWLP (solid curve). Both curves have CSC, laser heating, and NC phases. The initial cryogen spurt for both SCS-SLP and MCS-MTWLP reduces the epidermal temperature by 45°C. Thereafter, a laser pulse heats the epidermis to a temperature close to the epidermal threshold damage temperature, $T_{TH,E}$ [32]. The laser pulse is followed by NC during SCS-SLP and the epidermal temperature decreases to 40°C after 50 milliseconds, which is still 4°C higher than the initial skin temperature. In contrast, the laser pulse is followed by another cryogen spurt during MCS-MTWLP and the epidermal temperature decreases by 65°C after 50 milliseconds, which is even greater than the initial temperature reduction because the CSC heat flux increases with initial epidermal temperature [6]. A second laser pulse with the same radiant exposure can then be applied without heating the epidermis to a temperature over $T_{TH,E}$.

As a representation of the intravascular core blood vessel temperature, we show in Figure 3b the temperature variations over time at the center of a vessel with a diameter of 150 μm for SCS-SLP (circles) and MCS-MTWLP (solid curve). For SCS-SLP, the blood temperature reaches only 75°C at the end of the laser pulse because light is strongly attenuated by blood. Subsequent heat diffusion from blood heats the center of the vessel to 91°C, which is still lower than the threshold photocoagulation temperature, $T_{TH,B}$. For MCS-MTWLP, although the blood temperature induced by the first TWLP is lower as compared to SLP, a much higher blood temperature is induced by the second TWLP because heat generated by the first pulse is partially preserved in the blood vessel. In summary, the MCS-MTWLP approach effectively protects the epidermis while at the same time achieving higher core intravascular temperatures over longer periods of time, which are expected to destroy larger blood vessels irreversibly.

Simulated Photocoagulation

To illustrate the overall effect of MCS-MTWLP on blood vessels of varying diameters, we present in Figures 4–6 the cross-sectional distributions of the damage parameter, Ω, for both SCS-SLP and MCS-MTWLP with different skin pigmentation, vessel sizes, and depths. Since an $\Omega \geq 1$ indicates tissue necrosis and blood vessel photocoagulation, red to yellow (white on black and white print) areas represent coagulated tissue and light blue (gray) areas represent native healthy skin. We assume further that blood coagulation of the entire vessel is required to induce irreversible damage [7]. For moderately pigmented skin, SCS-SLP can induce irreversible damage to blood vessels with diameters up to 110 μm (Fig. 4a) when the vessel depth is 300 μm. In contrast, MCS-MTWLP can induce irreversible damage to blood vessels up to 150 μm in diameter (Fig. 4b).

When the vessel depth is 800 μm, SCS-SLP can induce irreversible damage to only those blood vessels with diameters up to 70 μm (Fig. 5a) due to light attenuation by the dermis. MCS-MTWLP can induce irreversible damage to blood vessels up to 90 μm in diameter (Fig. 5b). If we assume methemoglobin is generated after the first laser pulse, the blood absorption coefficient at 1,064 nm increases by a factor of three, and the scattering coefficient also increases due to the transition of erythrocytes from a biconcave to spheroidal shape [16,33]. Using these optical properties for the second laser pulse, MCS-MTWLP can then induce irreversible damage to blood vessels up to 150 μm in diameter (Fig. 5c). For darkly pigmented skin and a vessel depth of 300 μm, SCS-SLP can induce irreversible

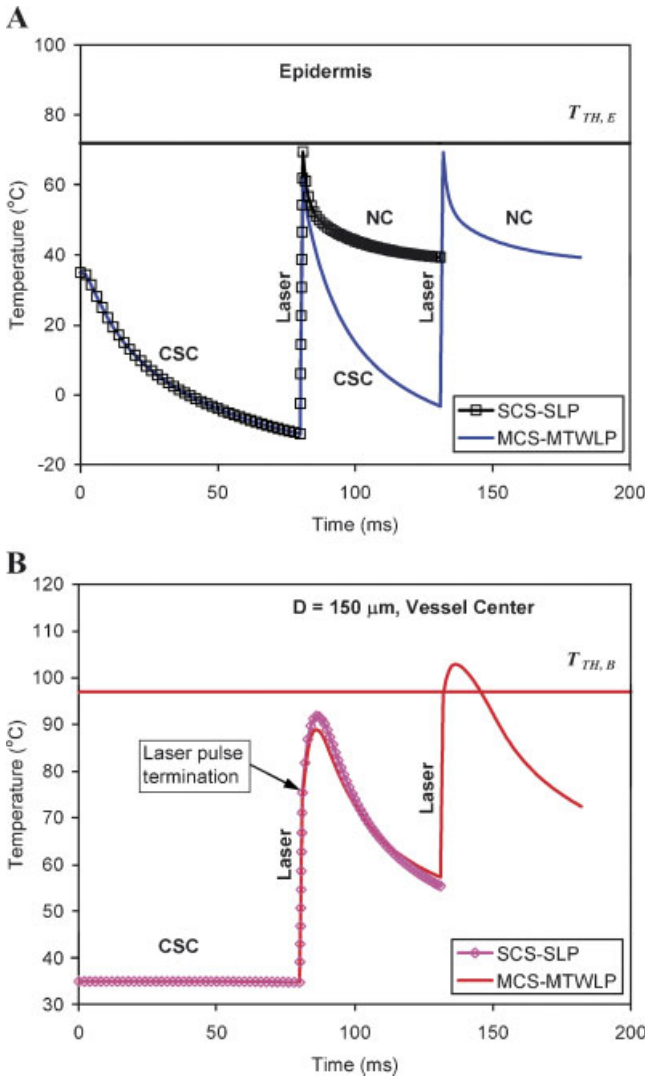

Fig. 3. Temperature variations over time within the epidermis (**a**) and center of 150 μm diameter vessel (**b**) with SCS-SLP and MCS-MTWLP. Moderately pigmented skin; blood vessel depth, 300 μm; SLP, 5 J/cm^2; MTWLP, 4 J/cm^2 532 nm+6 J/cm^2 1,064 nm, repetition rate, 20 Hz. [Figure can be viewed in color online via www.interscience.wiley.com.]

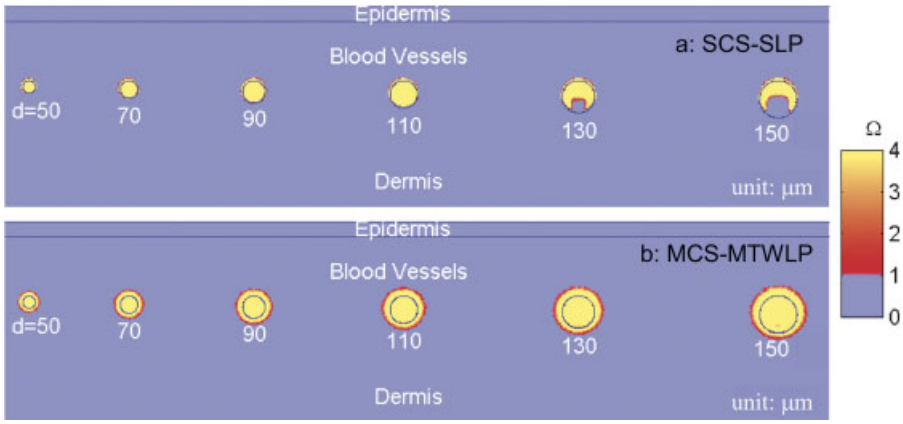

Fig. 4. Color maps of calculated Ω values for SCS-SLP (**a**) and MCS-MTWLP (**b**). Moderately pigmented skin; blood vessel depth, 300 μm; SLP, 5 J/cm^2; MTWLP, 4 J/cm^2 532 nm+6 J/cm^2 1,064 nm, repetition rate, 20 Hz. [Figure can be viewed in color online via www.interscience.wiley.com.]

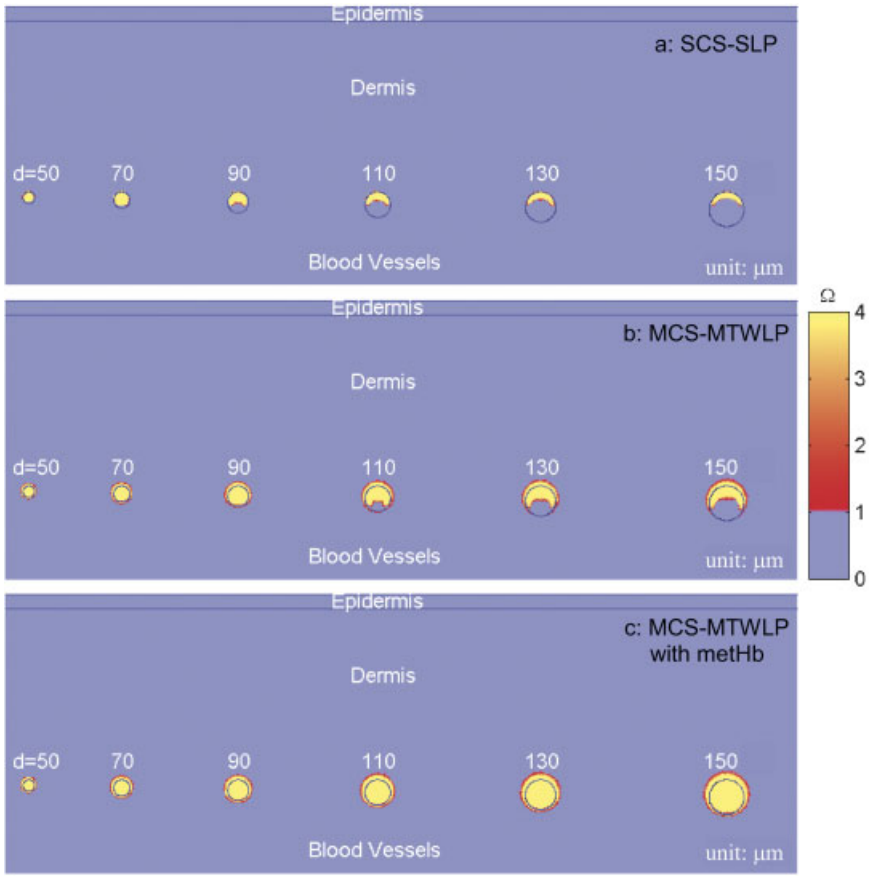

Fig. 5. Color maps of calculated Ω values for SCS-SLP (**a**), MCS-MTWLP (**b**), and MCS-MTWLP with methemoglobin formation (**c**). Moderately pigmented skin; blood vessel depth, 800 μm; SLP, 5 J/cm^2; MTWLP, 4 J/cm^2 532nm+6 J/cm^2 1,064 nm, repetition rate, 20 Hz. [Figure can be viewed in color online via www.interscience.wiley.com.]

damage to blood vessels with diameters up to 90 μm (Fig. 6a) due to the lower threshold radiant exposure (4 J/cm^2 as compared to 5 J/cm^2 for moderately pigmented skin) and more light absorption in the epidermis. MCS-MTWLP can induce irreversible damage to blood vessels up to 110 μm in diameter (Fig. 6b). If we assume methemoglobin is generated after the first laser pulse, MCS-MTWLP can then induce irreversible damage to blood vessels up to 150 μm in diameter (Fig. 6c). It should be noted that the coagulated areas with MCS-MTWLP are larger than the vessel diameter because of higher heat diffusion into the dermis during MCS-MTWLP. Perivascular coagulation may be necessary to denature the vessel wall and eliminate the vessel completely.

Photocoagulation of In Vivo RWCM Blood Vessels

To quantify the actual physiological responses of blood vessels to MCS-MTWLP, experiments were conducted in the RWCM. The procedures were MTWLP at a repetition rate of 27 Hz, SLP, and multiple exposures of SLP. The interval between SLP exposures was 5 minutes. CSC was not applied since the laser irradiation was from the dermal side of the RWCM. Because we were interested in venous and capillary malformations, venules were selected for laser irradiation. Typical structural and functional changes of RWCM blood vessels in response to MTWLP and SLP are shown in Figure 7.

Figure 7a shows the subdermal side of a RWCM before laser irradiation. Two venules with diameters of 156 and 154 μm were selected for MTWLP and SLP, respectively. The MTWLP sequence consisted of five pulses. Each pulse had a 1 millisecond duration, 3 J/cm^2 radiant exposure at 532 nm, and 5.4 J/cm^2 radiant exposure at 1,064 nm. The SLP had a 1 millisecond duration, 4 J/cm^2 radiant exposure at 532 nm. The immediate structural changes of blood vessels in response to MTWLP and SLP are shown in Figure 7b. With MTWLP, the irradiated blood vessel became significantly constricted. With SLP, no apparent changes were noted.

Figure 7c shows a map of the blood flow in the RWCM before laser irradiation obtained with LSI. The color scale on the right indicates relative blood flow. The camera exposure time was 10 milliseconds and the map is an average of 30 frames. Figure 7d shows the blood flow image immediately after laser irradiation, and provides crucial

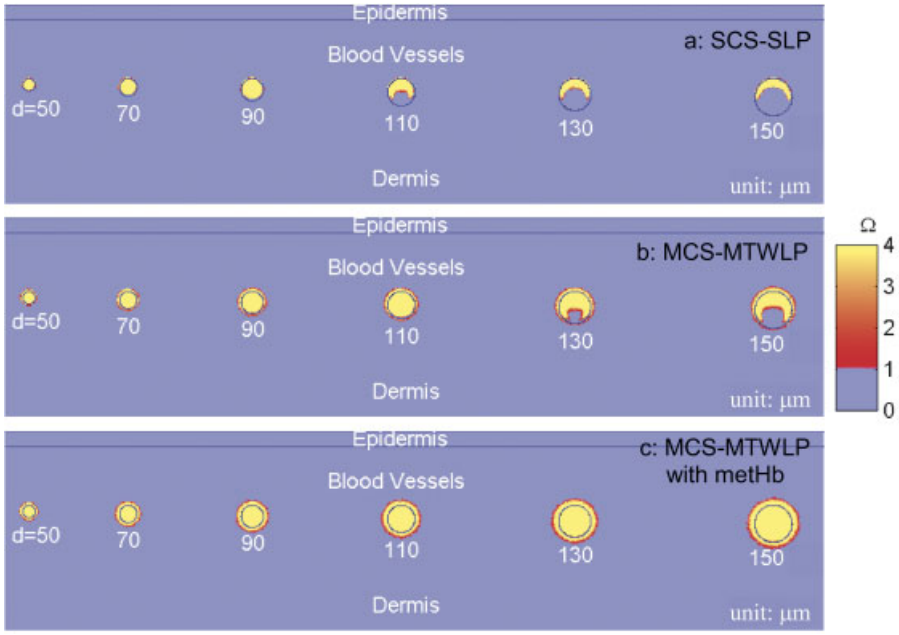

Fig. 6. Color maps of calculated Ω values for SCS-SLP (**a**), MCS-MTWLP (**b**), and MCS-MTWLP with methemoglobin formation (**c**). Darkly pigmented skin; blood vessel depth, 300 μm; SLP, 4 J/cm^2; MTWLP, 3.5 J/cm^2 532 nm+6 J/cm^2 1,064 nm, repetition rate, 20 Hz. [Figure can be viewed in color online via www.interscience.wiley.com.]

evidence that blood flow was completely stopped in the vessel irradiated by MTWLP. In contrast, blood flow was readily apparent in the vessel irradiated with SLP. This animal was observed for 1 week after laser irradiation and no recanalization or reperfusion of the blood vessels exposed to MTWLP occurred. No ulceration of the subdermis was observed on sites receiving either MTWLP or SLP. These data suggest that the MTWLP has significant advantages over SLP by inducing irreversible damage of larger blood vessels without adverse effects.

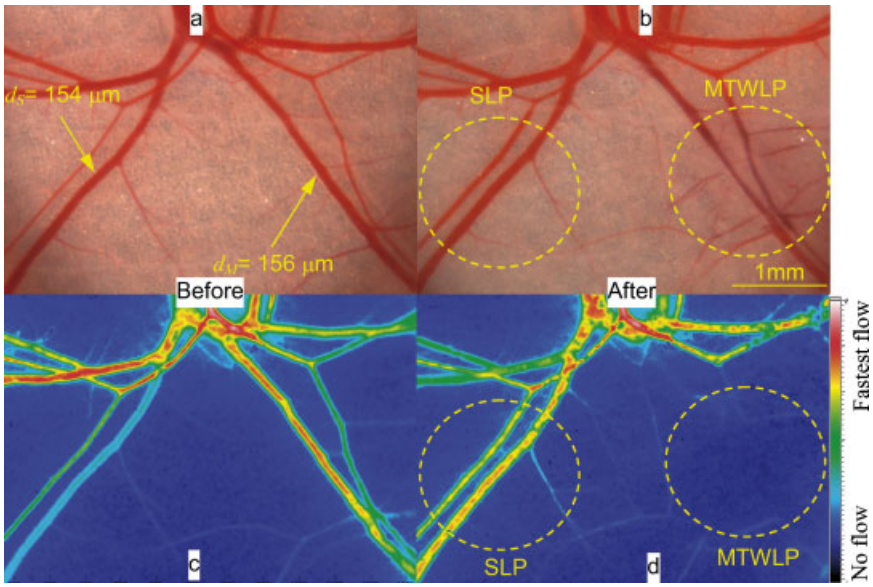

Fig. 7. Structural and functional changes of hamster RWCM blood vessels induced by SLP (4 J/cm^2 532 nm) and MTWLP (five pulses, 27 Hz, 3 J/cm^2 532 nm+5.4 J/cm^2 1,064 nm per pulse). **a**: Color image of the chamber before laser irradiation. **b**: Color image immediately after laser irradiation. **c**: Speckle flow image before laser irradiation. **d**: Speckle flow image immediately after laser irradiation. [Figure can be viewed in color online via www.interscience.wiley.com.]

Six blood vessels were irradiated by MTWLP and seven vessels by SLP. For MTWLP with a repetition rate of 27 Hz and five pulses in total, the threshold radiant exposure (532 nm) to induce irreversible blood vessel damage (~150 μm diameter) is 3 J/cm^2 per pulse. For SLP, 5 J/cm^2 per pulse is not sufficient to induce irreversible blood vessel damage. However, the blood vessel can be photocoagulated with five exposures of SLP of 5 J/cm^2 per pulse at an interval of 5 minutes. This is somewhat surprising because heat accumulation in the blood vessel after 5 minutes should be negligible. Likely, microscopic damage accumulates which contributes to blood vessel photocoagulation and clot formation with multiple exposures of SLP [34]. Further experiments are needed to elucidate the effect of multiple exposures of SLP.

DISCUSSION

Our simulations indicate that the risk of epidermal injury with MCS-MTWLP is not higher as compared to SCS-SLP for two reasons: (1) the 532 nm radiant exposure in MCS-MTWLP is lower as compared to SCS-SLP; and (2) CSC is able to extract more heat from the epidermis when the latter is heated to an elevated temperature by the first pulse. Without active skin cooling by cryogen spray between laser pulses, it is not possible to deliver the second pulse without damaging the epidermis. The numerical results also show that the addition of the 1,064 nm wavelength does induce bulk dermal heating which reduces the required light dosage at 532 nm to induce blood vessel photocoagulation. However, for deep blood vessels and/or darkly pigmented skin, bulk dermal heating and multiple laser pulses are insufficient to induce photocoagulation of large blood vessels. Fortunately, due to the enhanced infrared absorption of blood resulting from methemoglobin formation after the first laser pulse, exposure to subsequent 1,064 nm irradiation can induce photocoagulation of large blood vessels.

In our simulations, the pulse interval between MCS-MTWLP was 49 milliseconds which was selected based on two factors. First, the pulse interval should ideally be shorter than the thermal relaxation time (τ_r) of the targeted blood vessels to achieve thermal confinement. τ_r can be defined as the time during which the vessel center's temperature is reduced to 50% of its value immediately after laser irradiation. Theoretically, τ_r is 11 milliseconds for a 150 μm diameter vessel when the center of the lumen is heated by a line source. However, when the same diameter vessel is irradiated with light that has diffused through the dermis, τ_r is 57 milliseconds according to our simulations (see Fig. 8). Figure 8 shows that the vessel lumen center's temperature increases after laser irradiation due to heat diffusion from the top of the vessel, which greatly prolongs τ_r. Second, the cooling time between laser pulses should be sufficient to protect the epidermis from thermal injury. Our simulations do not show any epidermal injury with a 49 milliseconds cooling time, which is widely used in clinical practice (e.g., 40 milliseconds spurt+10 milliseconds delay or 30 milliseconds spurt+20 milliseconds delay).

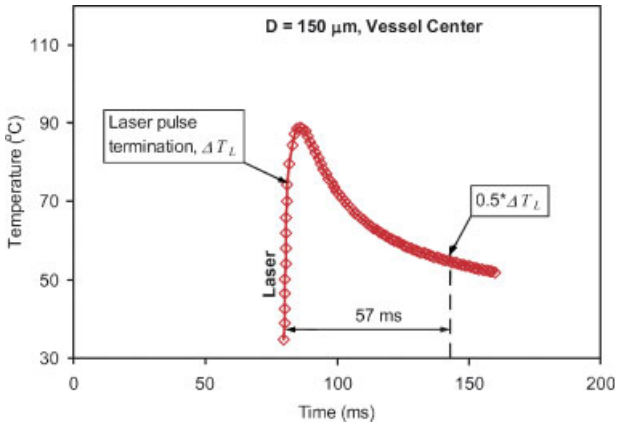

Fig. 8. Thermal relaxation of a 150 μm diameter vessel after laser irradiation, depth 300 μm. [Figure can be viewed in color online via www.interscience.wiley.com.]

In our studies, the combination of 532 and 1,064 nm wavelengths was selected because both can be generated by one device. Nevertheless, other wavelength combinations, such as 595/1,064 nm, might also be beneficial. In fact, a 595 nm wavelength is a better choice to treat large vessels because the light can penetrate deeper into blood. However, the combination of 595/1,064 nm requires two different types of lasers.

Our numerical results show that the temperature at the top portion of the blood vessel is maintained at T_B for both SLP and MTWLP. The reason is that significant water vaporization in blood is assumed to occur at T_B. Although the actual T_B is unknown, it is likely higher than what we assumed because of the very high heating rate and pressure increase in confined vessels [13]. In fact, higher T_B would favor the MCS-MTWLP approach because higher blood temperatures could be achieved with MTWLP before it reaches T_B. Previous studies have suggested that blood optical properties change with temperature [16,35], which is not considered with current models. Our approach is to assume that all hemoglobin is converted to methemoglobin after the first laser pulse because the transformation temperature between the two occurs at 60°C [16] which is lower than the simulated blood temperature. Further animal experiments with multiple 532 nm laser pulses are pending to elucidate the contribution of the 1,064 nm wavelength to blood vessel photocoagulation.

Our animal study shows that blood vessels constricted immediately after MTWLP irradiation at the threshold radiant exposure (Fig. 7b). With higher radiant exposure, blood vessels irradiated with MTWLP disappeared completely. Similar phenomena were observed by Suthamjariya et al. [36] during laser irradiation of hamster cheek pouch blood vessels with either 532 or 1,064 nm laser pulses of 10 milliseconds or longer. The authors found that immediate disappearance of a target vessel typically occurs before cavitation, which may be caused by contraction of an intravascular blood coagulum or perivascular collagen after thermal denaturation. They also suggested that immediate

vessel disappearance without hemorrhage is a useful clinical endpoint associated with good clinical results.

CONCLUSIONS

Using numerical and animal models, we demonstrated the potential advantages of MCS-MTWLP over SCS-SLP. The numerical simulations show that the MCS-MTWLP approach can provide sufficient epidermal protection while at the same time achieving photocoagulation of larger blood vessels as compared to SCS-SLP. Animal experiments show that the MTWLP can induce irreversible damage of larger blood vessels without adverse effects at the same or lower radiant exposure per pulse as compared to SLP. We believe that MCS-MTWLP may be a promising approach to improve therapeutic outcome for patients whose lesions feature large blood vessels, which can be confirmed by clinical and histological studies.

ACKNOWLEDGMENTS

The authors wish to thank Dr. Boris Majaron for significant discussions regarding this research and Cynthia Kim for her assistance with the animal surgery. This work was supported by the National Institutes of Health (GM 62177, AR 48458, and AR 47551 to JSN, HD42057 to GA, and P41-RR01192, Laser Microbeam and Medical Program), American Cancer Society (ACS-IRG 98-279-04 to BC), and UCR Academic Senate Grant (GA). Institutional support from the Beckman Laser Institute Endowment is also acknowledged. The prototype laser used in the animal experiments is on loan from Fotona, Ljubljana, Slovenia.

REFERENCES

1. Nelson JS, Milner TE, Anvari B, Tanenbaum BS, Kimel S, Svaasand LO, Jacques SL. Dynamic epidermal cooling during pulsed laser treatment of port-wine stain: A new methodology with preliminary clinical evaluation. Arch Dermatol 1995;131(6):695–700.
2. Nelson JS, Milner TE, Anvari B, Tanenbaum BS, Svaasand LO, Kimel S. Dynamic epidermal cooling in conjunction with laser-induced photothermolysis of port wine stain blood vessels. Lasers Surg Med 1996;19(2):224–229.
3. Chang CJ, Nelson JS. Cryogen spray cooling and higher fluence pulsed dye laser treatment improve port-wine stain clearance while minimizing epidermal damage. Dermatol Surg 1999;25(10):767–772.
4. Lanigan SW. Port-wine stains unresponsive to pulsed dye laser: Explanations and solutions. Br J Dermatol 1998; 139(2):173–177.
5. Lucassen GW, Svaasand LO, Verkruysse W, van Gemert MJC. Laser energy threshold for thermal vascular injury in a port-wine stain skin model. Lasers Med Sci 1995;10(4):231–234.
6. Jia W, Aguilar G, Nelson JS. Heat transfer dynamics during treatment of port wine stain birthmarks with multiple-intermittent cryogen spurts and laser pulses. 2005. ASME Summer Heat Transfer Conference July 17–22, 2005; San Francisco, CA.
7. Hohenleutner U, Hilbert M, Wlotzke U, Landthaler M. Epidermal damage and limited coagulation depth with the flashlamp-pumped pulsed dye-laser—a histochemical-study. J Invest Dermatol 1995;104(5):798–802.
8. Tan OT. Pulsed dye laser treatment of adult port-wine stains. In: Tan OT, editor. Management and treatment of benign cutaneous vascular lesions. Philadelphia: Lea & Febiger; 1992. pp 83–99.
9. Goldman MP, Fitzpatrick RE. Treatment of cutaneous vascular lesions. In: Goldman MP, Fitzpatrick RE, editors. Cutaneous laser surgery. St. Louis: Mosby; 1994. pp 19–105.
10. Selim MM, Kelly KM, Nelson JS, Wendelschafer-Crabb G, Kennedy WR, Zelickson BD. Confocal microscopy study of nerves and blood vessels in untreated and treated port wine stains: Preliminary observations. Dermatol Surg 2004;30(6): 892–897.
11. Verkruysse W, van Gemert MJC, Smithies DJ, Nelson JS. Modelling multiple laser pulses for port wine stain treatment. Phys Med Biol 2000;45(22):N197–N203.
12. Aguilar G, Diaz SH, Lavernia EJ, Nelson JS. Cryogen spray cooling efficiency: Improvement of port wine stain laser therapy through multiple-intermittent cryogen spurts and laser pulses. Lasers Surg Med 2002;31(1):27–35.
13. Jia W, Aguilar G, Verkruysse W, Franco W, Nelson JS. Improvement of port wine stain laser therapy by skin preheating prior to cryogen spray cooling: A numerical simulation. Lasers Surg Med 2005;38(2):155–162.
14. Mordon S, Brisot D, Fournier N. Using a "non uniform pulse sequence" can improve selective coagulation with a Nd: YAG Laser (1.06 μm): Thanks to met-hemoglobin absorption: A clinical study on blue leg veins. Lasers Surg Med 2003;32(2):160–170.
15. Fournier N, Brisot D, Mordon S. Treatment of leg telangiectases with a 532 nm KTP laser in multipulse mode. Dermatol Surg 2002;28(7):564–571.
16. Black JF, Barton JK. Chemical and structural changes in blood undergoing laser photocoagulation. Photochem Photobiol 2004;80(1):89–97.
17. Verkruysse W, Pickering JW, Beek JF, Keijzer M, van Gemert MJC. Modeling the effect of wavelength on the pulsed dye laser treatment of port wine stains. Appl Opt 1993;32(4):393–398.
18. Svaasand LO, Norvang LT, Fiskerstrand EJ, Stopps EKS, Berns MW, Nelson JS. Tissue parameters determining the visual appearance of normal skin and port-wine stains. Lasers Med Sci 1995;10(1):55–65.
19. Hillenkamp F. Interaction between laser radiation and biological systems. In: Hillenkamp F, Pratesi R, Sacci C, editors. Lasers in biology and medicine. New York: Plenum Press; 1979. pp 57–61.
20. Ma XY, Lu JQ, Ding HF, Hu XH. Bulk optical parameters of porcine skin dermis at eight wavelengths from 325 to 1557 nm. Opt Lett 2005;30(4):412–414.
21. Bashkatov AN, Genina EA, Kochubey VI, Tuchin VV. Optical properties of human skin, subcutaneous and mucous tissues in the wavelength range from 400 to 2000 nm. J Phys D Appl Phys 2005;38(15):2543–2555.
22. Wray S, Cope M, Delpy DT, Wyatt JS, Reynolds EOR. Characterization of the near-infrared absorption-spectra of cytochrome-aa3 and hemoglobin for the non-invasive monitoring of cerebral oxygenation. Biochim Biophys Acta 1988;933(1):184–192.
23. Reynolds L, Johnson C, Ishimaru A. Diffuse reflectance from a finite blood medium—applications to modeling of fiber optic catheters. Appl Opt 1976;15(9):2059–2067.
24. Welch AJ, Wissler EH, Priebe LA. Significance of blood-flow in calculations of temperature in laser irradiated tissue. IEEE Trans Biomed Eng 1980;27(3):164–166.
25. Weaver JA, Stoll AM. Mathematical model of skin exposed to thermal radiation. Aerosp Med 1969;40(1):24–30.
26. Lepock JR, Frey HE, Bayne H, Markus J. Relationship of hyperthermia-induced hemolysis of human-erythrocytes to the thermal-denaturation of membrane-proteins. Biochim Biophys Acta 1989;980(2):191–201.
27. Gourgouliatos ZF, Welch AJ, Diller KR, Aggarwal SJ. Laser-irradiation-induced relaxation of blood vessels in vivo. Lasers Surg Med 1990;10(6):524–532.
28. Mordon S, Desmettre T, Devoisselle J, Soulie S. Thermal damage assessment of blood vessels in a hamster skin flap

model by fluorescence measurement of a liposome-dye system. Lasers Surg Med 1997;20(2):131–141.
29. Barton JK, Rollins A, Yazdanfar S, Pfefer TJ, Westphal V, Izatt JA. Photothermal coagulation of blood vessels: A comparison of high-speed optical coherence tomography and numerical modeling. Phys Med Biol 2001;46(6):1665–1678.
30. Choi B, Kang NM, Nelson JS. Laser speckle imaging for monitoring blood flow dynamics in the in vivo rodent dorsal skin fold model. Microvasc Res 2004;68(2):143–146.
31. Choi B, Jia W, Channual J, Kelly KM, Lotfi J. The importance of long-term monitoring to evaluate the microvascular response to light-based therapies. J Invest Dermatol (in press).
32. Jacques SL, McAuliffe DJ. The melanosome—threshold temperature for explosive vaporization and internal absorption-coefficient during pulsed laser irradiation. Photochem Photobiol 1991;53(6):769–775.
33. Black JF, Wade N, Barton JK. Mechanistic comparison of blood undergoing laser photocoagulation at 532 and 1,064 nm. Lasers Surg Med 2005;36(2):155–165.
34. Tanghetti E, Sherr EA, Sierra R, Mirkov M. The effects of pulse dye laser double-pass treatment intervals on depth of vessel coagulation. Lasers Surg Med 2006;38 (1):16–21.
35. Nilsson AMK, Lucassen GW, Verkruysse W, AnderssonEngels S, van Gemert MJC. Changes in optical properties of human whole blood in vitro due to slow heating. Photochem Photobiol 1997;65(2):366–373.
36. Suthamjariya K, Farinelli WA, Koh W, Anderson RR. Mechanisms of microvascular response to laser pulses. J Invest Dermatol 2004;122(2):518–525.